JOURNAL OF GEOPHYSICAL RESEARCH – SOLID EARTH, 105 (B4): 7893-7908

Viscoplastic self-consistent and equilibrium-based modeling of olivine lattice preferred orientations: Implications for the upper mantle seismic anisotropy

Andréa Tommasi and David Mainprice

Laboratoire de Tectonophysique, ISTEEM, CNRS/Université de Montpellier II, Montpellier, France

Gilles Canova[1]

Laboratoire de Génie Physique et Mécanique des Matériaux, CNRS/ENSPG, St. Martin d'Hères, France

Yvan Chastel

Centre de Mise en Forme de Matériaux, Ecole de Mines de Paris, Sophia Antipolis, France

Abstract. Anisotropy of upper mantle physical properties results from lattice preferred orientation (LPO) of upper mantle minerals, in particular olivine. We use an anisotropic viscoplastic self-consistent (VPSC) and an equilibrium-based model to simulate the development of olivine LPO and, hence, of seismic anisotropy during deformation. Comparison of model predictions with olivine LPO of naturally and experimentally deformed peridotites shows that the best fit is obtained for VPSC models with relaxed strain compatibility. Slight differences between modeled and measured LPO may be ascribed to activation of dynamic recrystallization during experimental and natural deformation. In simple shear, for instance, experimental results suggest that dynamic recrystallization results in further reorientation of the LPO leading to parallelism between the main (010)[100] slip system and the macroscopic shear. Thus modeled simple shear LPOs are slightly misoriented relative to LPOs measured in natural and experimentally sheared peridotites. This misorientation is higher for equilibrium-based models. Yet seismic properties calculated using LPO simulated using either anisotropic VPSC or equilibrium-based models are similar to those of naturally deformed peridotites; errors in the prediction of the polarization direction of the fast S wave and of the fast propagation direction for P waves are usually < 15°. Moreover, overestimation of LPO intensities in equilibrium-based and VPSC simulations at high strains does not affect seismic anisotropy estimates, because these latter are weakly dependent on the LPO intensity once a distinct LPO pattern has been developed. Thus both methods yield good predictions of development of upper mantle seismic anisotropy in response to plastic flow. Two notes of caution have nevertheless to be observed in using these results: (1) the dilution effect of other upper mantle mineral phases, in particular enstatite, has to be taken into account in quantitative predictions of upper mantle seismic anisotropy, and (2) LPO patterns from a few naturally deformed peridotites cannot be reproduced in simulations. These abnormal LPOs represent a small percent of the measured natural LPOs, but the present sampling may not be representative of their abundance in the Earth's upper mantle.

1. Introduction

Olivine is by far the most abundant (~ 60-70%) and the weakest upper mantle mineral under a wide range of deformation conditions, as shown by experimental studies [e.g., *Bai et al.*, 1991; *Mackwell*, 1991] and analysis of naturally deformed peridotites [*Nicolas and Poirier*, 1976]. Olivine crystals are elastically [*Kumazawa and Anderson*, 1969], thermally [*Schärmeli*, 1982], and mechanically anisotropic [*Bai et al.*, 1991]. Thus, if olivine lattice preferred orientations (LPOs) develop during flow, the upper mantle should display anisotropic seismic, thermal, and mechanical properties. Indeed, seismic anisotropy measurements, particularly shear wave splitting, have been extensively used in recent years as a tool to unravel upper mantle flow patterns [e.g., *Russo and Silver*, 1994; *Silver and Chan*, 1988; *Vauchez and Barruol*, 1996; *Vinnik et al.*, 1984].

Olivine LPO forms through crystal reorientation during dislocation creep-dominated deformation [*Nicolas and Christensen*, 1987]. There is hence a link between the deformation accommodated within the upper mantle, LPO of upper mantle rock-forming minerals, and seismic anisotropy. The relationship between LPO and the elastic properties of upper mantle rocks is well established [*Babuska*, 1972; *Carter et al.*, 1972; *Christensen*, 1984; *Nicolas and Christensen*, 1987]. The seismic properties of an aggregate may be calculated as a weighted average of the elastic properties of its constituent crystals; they depend directly on the LPO [e.g., *Mainprice and Silver*, 1993]. On the other hand, the relationship between upper mantle deformation and olivine lattice preferred orientations is still poorly constrained.

Analysis of naturally and experimentally deformed upper mantle rocks allows the determination of the LPO patterns that may develop during plastic deformation. Yet a quantitative relationship

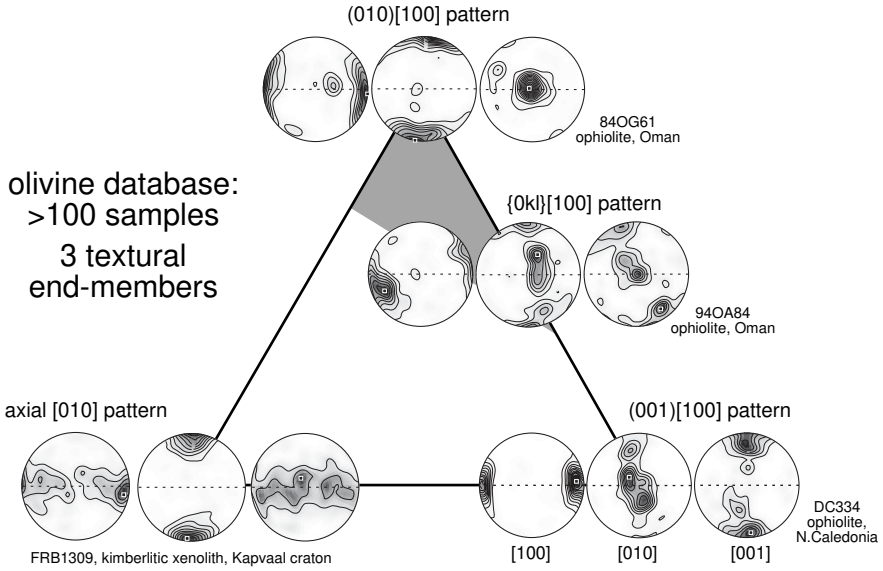

Figure 1. Typical olivine lattice preferred orientations measured in peridotites deformed under the high-temperature, low-stress conditions prevailing in the upper mantle represented as continuum variations between (010)[100], (001)[100], and axial [010] patterns. Ninety percent of the naturally deformed peridotites in the database show either (010)[100] or {0kl}[100] patterns and plot in the gray area of the diagram. Lower hemisphere equal-area projections are shown: 100 grains or more, contours at 1 m.u.d. (multiple of an uniform distribution) intervals. Inverse-log shading varies from white (minimum density) to black (maximum density, also indicated by a solid square). Dashed lines mark the foliation; lineation is horizontal.

between strain and LPO intensity cannot be established, because natural peridotites lack strain markers allowing a strain quantification and experiments are usually limited to a few percent strain. Moreover, strain paths in natural deformation are generally unknown, and experiments are restricted to a few simple deformation paths (axial compression, plane compression, and simple shear). On the other hand, numerical models of LPO evolution with progressive deformation of a polycrystalline aggregate offer an insight into how LPO development is influenced by the activity of available slip systems, their critical resolved shear stress, deformation path, and finite strain. They also offer the possibility of predicting the LPO, and thus the upper mantle anisotropy, associated with a specific upper mantle flow process [e.g., *Tommasi et al.*, 1999]. However, these models simulate deformation by dislocation glide only. Their predictive value depends therefore on how much olivine LPO patterns are affected by other deformation mechanisms, such as dynamic recrystallization.

Analysis of naturally deformed peridotites suggests that under deformation conditions prevailing in the first 200 km of the upper mantle olivine deforms essentially by an association of dislocation creep (dislocation glide and climb) and dynamic recrystallization (by nucleation, subgrain rotation, or grain boundary migration) [e.g., *Avé-Lallemant*, 1967; *Boudier and Coleman*, 1981; *Boullier and Nicolas*, 1975; *Green and Radcliffe*, 1972; *Mercier and Nicolas*, 1975; *Nicolas et al.*, 1971; *Skrotzki et al.*, 1990]. LPO evolution during upper mantle deformation should result from interactions between these deformation mechanisms. Yet compilation of olivine LPOs from 120 natural peridotites [*Ben Ismail and Mainprice*, 1998] shows that in spite of variations in deformation conditions, strain histories, and postdeformational evolutions from one sample to another, few distinct LPO patterns develop (Figure 1). Ninety-five percent of the samples display LPO patterns that may be interpreted as resulting from dislocation glide on {0kl}[100] systems, of which the most active is (010)[100], with subsidiary activation of (010)[001]. This suggests that, although dynamic recrystallization processes may affect LPO development [*Urai et al.*, 1986], olivine LPO patterns are essentially controlled by dislocation glide. This inference is corroborated by the analysis of olivine LPO in experimentally deformed dunites [*Avé-Lallemant*, 1975; *Nicolas et al.*, 1973; *Zhang and Karato*, 1995]. Highly recrystallized samples have LPO patterns similar, but not identical, to those of less recrystallized samples. These observations suggest that numerical models may bear reasonable first-order predictions of LPO development during natural deformation. These models also offer an insight on how the aggregate strength depends on the active slip systems and thus on the orientation of the grains. They allow therefore an investigation of the mechanical anisotropy induced by an evolving LPO (A. Tommasi et al., manuscript 2000).

In this paper, we present numerical models of olivine LPO development using both an anisotropic self-consistent viscoplastic approach [*Lebensohn and Tomé*, 1993] and a stress equilibrium-based model [*Chastel et al.*, 1993]. These two approaches were selected because they may be coupled to large-scale flow models in order to predict the development of seismic anisotropy in the upper mantle [*Blackman and Kendall*, 1997; *Blackman et al.*, 1996; *Chastel et al.*, 1993; *Tommasi*, 1998; *Tommasi et al.*, 1999]. Modeling results are then compared to LPOs of naturally and experimentally deformed upper mantle rocks. The reliability of upper mantle seismic anisotropy predictions using olivine LPOs calculated using both approaches is accessed through the comparison of seismic properties calculated for modeled aggregates to those of naturally deformed peridotites.

2. Modeling LPO Development in Polycrystals

In the last two decades, LPO evolution in deforming olivine polycrystals has been simulated using purely kinematic [*Etchecopar*, 1977; *Etchecopar and Vasseur*, 1987; *Ribe*, 1989], relaxed-constraints Taylor or similar [*Ribe and Yu*, 1991; *Takeshita*, 1989; *Takeshita et al.*, 1990], equilibrium-based [*Blackman*

et al., 1996; *Chastel et al.*, 1993], constrained-hybrid [*Parks and Ahzi*, 1990], isotropic [*Takeshita et al.*, 1990] and "*n*-site" [*Wenk et al.*, 1991] viscoplastic self-consistent approaches, and two-dimensional finite difference models [*Zhang et al.*, 1994]. All these polycrystal plasticity models are based on the assumption that crystal reorientation and LPO development are controlled by intracrystalline slip on a few crystallographic planes. In addition, with the exception of kinematic and finite difference models, they all assume that the polycrystal behavior may be calculated by an appropriate average of the microscopic (grain) responses; the lower and upper bounds are represented by the stress equilibrium [*Chastel et al.*, 1993] and *Taylor* [1938] models, which impose homogeneous stress or strain within the aggregate.

Dynamic recrystallization has been taken into account in a few models [*Etchecopar*, 1977; *Etchecopar and Vasseur*, 1987; *Jessel*, 1988; *Wenk et al.*, 1997]. All these models predict a similar LPO for simple shear deformation: a single maxima pattern in which the main slip system parallels the macroscopic shear. However, their physical bases are completely different. This highlights the fact that dynamic recrystallization is a poorly known process. Some fundamental questions still need to be answered: (1) Which grains tend to recrystallize preferentially? (2) Which are the orientation relationships between recrystallized and parent grains? (3) Variations in internal energy between neighboring grains control the grain boundary migration, but do grains in easy slip orientations display lower or higher internal energy than those in hard orientations? Can this relationship vary with temperature?

Another unsolved question is which recrystallization mechanism predominates during upper mantle deformation. Microstructures characteristic of both subgrain rotation and grain boundary migration are observed in naturally deformed peridotites. However, preponderance of porphyroclastic microstructures within the Laboratoire de Tectonophysique's database [*Ben Ismail and Mainprice*, 1998] suggests that subgrain rotation, a mechanism that has been overlooked in recent recrystallization models [*Wenk et al.*, 1997], may play a dominant role.

Thus we choose to use deformation models to predict LPO development and the evolution of seismic properties of olivine polycrystals. We selected the equilibrium-based approach [*Chastel et al.*, 1993] and the viscoplastic self-consistent model (VPSC) [*Lebensohn and Tomé*, 1993] because they rely on robust physical assumptions and are fast enough to be coupled to large-scale flow models. The bias introduced in the predictions by the nonsimulation of dynamic recrystallization is evaluated by a careful comparison of the modeled LPO with LPO measured in naturally and experimentally deformed peridotites. In the next paragraphs we briefly review the principles of the two models. A more complete description is given by *Chastel et al.* [1993], *Lebensohn and Tomé* [1993], and *Tomé and Canova* [1998].

In both models, at the grain scale, deformation takes place when a slip system becomes active. The shear rate in a slip system s is related to the local deviatoric stress tensor $\underline{\underline{s}}$ by a viscoplastic law:

$$\dot{\gamma}^s = \dot{\gamma}_0 \left(\frac{\tau_r^s}{\tau_0^s} \right)^{n^s} = \dot{\gamma}_0 \left(\frac{r_j^s s_j}{\tau_0^s} \right)^{n^s}, \qquad (1)$$

where $\dot{\gamma}_0$ is a reference strain rate, taken as 1 s^{-1}, and n^s, τ_r^s, and τ_0^s are the stress exponent, the resolved shear stress, and the critical resolved shear stress, respectively, for the system s, whose orientation relative to the macroscopic axes is expressed by its Schmid tensor $\underline{\underline{r}}^s$. The sum of the shear rates over all slip systems gives the grain's strain rate $\dot{\underline{\underline{\varepsilon}}}$.

The microscopic constitutive relation is known. The problem lies therefore in the calculation of a microscopic state ($\underline{\underline{s}}$, $\dot{\underline{\underline{\varepsilon}}}$) for each grain, whose volume average (denoted by angle brackets) determines the response of the polycrystal ($\underline{\underline{\Sigma}}$, $\dot{\underline{\underline{E}}}$):

$$\left\langle \underline{\underline{s}} \right\rangle = \underline{\underline{\Sigma}}, \qquad \left\langle \dot{\underline{\underline{\varepsilon}}} \right\rangle = \dot{\underline{\underline{E}}}. \qquad (2)$$

Both models are statistical approaches: They do not account for the precise topology of the aggregate. In the equilibrium-based model we consider that all crystals experience the same state of stress. Strain compatibility is only fulfilled at the aggregate scale (i.e., in an average sense). Within the VPSC model the microscopic stress and strain rate may differ from the corresponding macroscopic quantities; both strain compatibility and stress equilibrium are ensured at the aggregate scale. In addition, the VPSC formulation explicitly accounts for the plastic anisotropy of the aggregate, which may be significant for materials with few slip systems, as olivine.

As a simplification, the original "one-site" model of *Molinari et al.* [1987] is used in the anisotropic VPSC formulation; influence of neighboring grains is not directly taken into account. Interactions between each grain and its surroundings are successively replaced by the interaction between an inclusion with similar lattice orientation and an infinite homogeneous equivalent medium (HEM), whose behavior is the weighted average of the behavior of all grains. This interaction problem is solved using the inclusion formalism of *Eshelby* [1957] (see review by *Lebensohn and Tomé* [1993]). Grain shape is assumed to be ellipsoidal, and the HEM is assumed to have a tangent behavior (linear approximation of the actual power law relation between stress and strain rate). This results in uniform strain rate and stress in each grain.

The *Eshelby* [1957] solution of the viscoplastic inclusion problem leads to an equation connecting local stresses and strain rates to the macroscopic quantities:

$$\dot{\varepsilon}_{ij} - \dot{E}_{ij} = -\alpha \tilde{M}_{ijkl} (s_{kl} - \Sigma_{kl}), \qquad (3)$$

where $\underline{\underline{\underline{\underline{\tilde{M}}}}}$ is the interaction tensor that depends on the rheological properties of the aggregate and on the grains' shape and α is a constant used to parameterize the interaction between grains and the HEM, i.e., to impose more or less stringent kinematic conditions on grains. A zero value of α corresponds to the Taylor model (the upper bound, not applicable to olivine because it displays less than five independent slip systems), a value of unity corresponds to the tangent VPSC model of *Lebensohn and Tomé* [1993], and an infinite value corresponds to the stress equilibrium model (the lower bound).

Numerical convergence is considered to be achieved when the relative difference between average and macroscopic quantities in (2) is lower than 0.03. Then, grain shapes are updated, and the reorientation of each grain is calculated. The lattice rotation rate for each grain (relative to the macroscopic axes) is given by

$$\omega_{ij} = \Omega_{ij} - \sum_s \tfrac{1}{2} \left(b_i n_j - b_j n_i \right)^s \dot{\gamma}^s + \tilde{\omega}_{ij}, \qquad (4)$$

where $\underline{\underline{\underline{\Omega}}}$ is the antisymmetric component of the imposed macroscopic velocity gradient $\underline{\underline{L}}$, the second term is the plastic spin of the grain, and $\underline{\underline{\underline{\tilde{\omega}}}}$ is the reorientation rate of the associated ellipsoidal inclusion, which depends on the difference in strain rate between the grain and the polycrystal and increases with ellipsoid distortion (i.e, with increasing deformation) [*Tiem et al.*, 1986]. This last term is not considered in the equilibrium-based model.

Thus, although VPSC models with $\alpha = 100$ approach the equilibrium-based model in terms of mechanical response, at high strains LPO evolutions predicted by the two models differ significantly.

For a given set of active slip systems, initial LPO, and microscopic rheological parameters n^s and τ_0^s both models calculate the evolution of the aggregate yield strength, the activity of slip systems, and the LPO development for a given macroscopic strain history. Within the following simulations, polycrystals are composed of 1000 grains. Before deformation, aggregates display random lattice preferred orientations, and grains are supposed spherical. The imposed velocity gradients are constant. They are given by

$$\mathbf{L} = \begin{bmatrix} 0.5 & 0 & 0 \\ 0 & -1 & 0 \\ 0 & 0 & 0.5 \end{bmatrix}, \quad \mathbf{L} = \begin{bmatrix} 1 & 0 & 0 \\ 0 & -1 & 0 \\ 0 & 0 & 0 \end{bmatrix}, \quad \mathbf{L} = \begin{bmatrix} 0 & 1 & 0 \\ 0 & 0 & 0 \\ 0 & 0 & 0 \end{bmatrix}, \quad (5)$$

for axial compression, pure shear, and simple shear simulations, respectively. The only tuning parameters are therefore the active slip systems for olivine, their critical resolved shear stresses, and stress exponents and the interaction between grains and the HEM, defined by α.

We use the Von Mises equivalent deviatoric stress S_{eq} and strain rate E_{eq} as scalar measures of the macroscopic deviatoric stress and strain rate:

$$S_{eq} = \sqrt{\frac{3}{2}\Sigma_{ij}\Sigma_{ij}}, \quad E_{eq} = \sqrt{\frac{2}{3}\dot{E}_{ij}\dot{E}_{ij}}, \quad (6)$$

and the time step dt is chosen so that each deformation step k leads to a 2.5% equivalent strain for the polycrystal

$$\varepsilon_{eq}^{k} = E_{eq}{}^{k} dt = 0.025 . \quad (7)$$

Grain orientations are characterized by the three Euler angles (φ_1, ϕ, φ_2) of *Bunge* [1982] that define the matrix **g** describing the rotation of the crystal from a standard (sample) orientation to its actual orientation. As given by *Mainprice and Silver* [1993], the strength of a LPO is characterized by the dimensionless texture index J [*Bunge*, 1982]

$$J = \int f(\mathbf{g})^2 d\mathbf{g} , \quad (8)$$

where f(**g**) is the orientation distribution function (ODF), which describes quantitatively the volume fraction of the sample with an orientation between **g** and d**g**. The J index varies between 1 (random LPO) and infinity (single crystal). In our work, however, it has a maximum of ~ 250 because we use the harmonic method and truncate the series at degree 22. Both the J index and the contouring of the stereoplots (in multiples of a uniform distribution) depend on the number of grains used to characterize the LPO, but this variation decreases with an increasing number of grains and becomes negligible for more than 100 grains. We may therefore compare the modeled LPOs (1000 grains) to those measured in peridotites (100 to 200 grains).

3. Olivine Slip Systems and Microscopic Rheological Parameters

Optical and transmission electron microscope observations of naturally and experimentally deformed peridotites as well as of single crystals deformed in different crystallographic orientations

Table 1. Olivine Slip Systems

Temperature	σ_1 Orientation	Dislocations	Slip Systems	Remarks	References
600°C	$[101]_c$	screw, **b** = [001]; edges very short	(?)[001]		1
800°C	$[101]_c$ and $[011]_c$	screw and edge, **b** = [001]	(100)[001], {110}[001], and (010)[001]		1
800°C	$[110]_c$	screw and edge, **b** = [010] screw and edge, **b** = [100]	(100)[010] (010)[100]	high-strain domains low-strain domains high flow stress (1.28 GPa)	1
1000°C	$[101]_c$	screw and edge, **b** = [001], some loops; fewer **b** = [100]	(100)[001], {110}[001], secondary (001)[100]		1
1000°C	$[011]_c$	screw and edge, **b** = [001], some loops	(010)[001]		1
1000°C	$[110]_c$	screw and edge, **b** = [100], some loops	(010)[100]	flow stress similar to $[101]_c$	1
> 1150°	$[101]_c$	screw and edge **b** = [100], screw segments longer than edge segments; few screw **b** = [001]; (100) subgrain boundaries	(001)[100], secondary (100)[001]	intermediate strength orientation at high temperature, it becomes the softest one at high f_{O_2}	2, 3
> 1150°	$[011]_c$	screw and edge, **b** = [001], loops of (010)[001]; screw **b** = [100], subgrain walls in (010); [100] organization	(010)[001] and (010)[100]	hardest orientation at high temperature	2, 3
> 1150°	$[110]_c$	screw and edge **b** = [100], numerous loops in the (010) plane; [100] organization	(010)[100]	softest orientation at high temperature	2, 3
> 1150°	$[110]_c$ and $[101]_c$		{031}[100], {021}[100], and {011}[100]?	only observed in forsterite	4

References: 1, Phakey et al. [1972]; 2, Durham and Goetze [1977] and Durham et al. [1977]; 3, Bai et al. [1991] and Bai and Kohlstedt [1992]; 4, Darot and Gueguen [1981].

(Table 1) show that olivine deforms essentially by slip on {0kl}[100] and {hk0}[001] systems, mainly (010)[100], (001)[100], (010)[001], (100)[001], and {110}[001] [e.g., *Bai and Kohlstedt*, 1992; *Doukhan et al.*, 1984; *Durham et al.*, 1977; *Goetze and Kohlstedt*, 1973; *Phakey et al.*, 1972; *Raleigh*, 1968]. Critical resolved shear stresses for these systems and, hence, their activity depend on temperature, stress (or strain rate), and water and oxygen fugacities [*Bai et al.*, 1991; *Darot and Gueguen*, 1981; *Durham and Goetze*, 1977; *Mackwell et al.*, 1985; *Phakey et al.*, 1972]. However, most naturally deformed peridotites display LPO typical of slip on high-temperature {0kl}[100] systems (Figure 1). LPO patterns suggesting high activity of low-temperature {hk0}[001] systems are restricted to mylonites that accommodate the low-temperature, high-stress deformation associated with the emplacement of peridotitic slices into the crust [e.g., *Boudier and Coleman*, 1981; *Garcia-San Millan*, 1998].

Thus in most models we use critical resolved shear stresses τ_0^s and stress exponent n^s values (Table 2) inferred from high-temperature experimental deformation of dry, orthopyroxene-buffered olivine single crystals [*Bai et al.*, 1991]. Under these deformation conditions the stress exponent is independent of loading orientation, stress level, temperature, and oxygen fugacity, with a constant value of 3.5 ± 0.1. Critical resolved shear stresses for the three main slip systems for olivine, (010)[100], (001)[100], and (010)[001], are deduced from the constitutive relations for crystals compressed in different orientations, considering that most of the deformation in each loading orientation is accommodated by the slip system displaying the highest Schmid factor. This assumption, although not exact, is partially justified by optical and TEM observations. Arbitrary higher critical resolved shear stresses are imposed on other known slip systems (Table 2).

Table 2. Slip System Data Used to Simulate High-Temperature Deformation

Slip System	Critical Resolved Shear Stress τ_0*	Stress Exponent n
(010)[100]	1	3.5
(001)[100]	1	3.5
(010)[001]	2	3.5
(100)[001]	3	3.5
{011}[100]	4	3.5
{031}[100]	4	3.5
{110}[001]	6	3.5
{111}[110]		
{111}[011]†	500	3.5

*Normalized relative to τ_0(010)[100].

†Since olivine displays only three independent slip systems, "complementary" pyramidal systems have to be used in the Taylor calculation of the initial solution (first iteration), but they are not used in the subsequent VPSC iterations.

Finally, latent hardening (due to dislocation interactions) is not considered in the following models, since work hardening is only observed in single crystals' deformation at 600°- 800°C [*Phakey et al.*, 1972]. At higher temperatures (≥1000°C), constant flow stress is attained after very low strains, probably because of activation of extensive cross-slip and climb [*Bai et al.*, 1991; *Durham and Goetze*, 1977; *Phakey et al.*, 1972]. Similarly, for olivine polycrystals, work hardening is restricted to experiments under dry conditions and temperatures below 1100°C [*Seront*, 1993].

4. LPO Evolution in Olivine Polycrystals: Anisotropic VPSC and Lower Bound Simulations

Figures 2 and 3 show LPOs obtained in axial compression, pure shear, and simple shear after 0.5 and 1.0 equivalent strains in one-site anisotropic VPSC and equilibrium-based simulations using the microscopic parameters listed in Table 2. During natural deformation, strain compatibility is partly ensured by activation of deformation mechanisms other than dislocation glide (e.g., climb [*Durham and Goetze*, 1977] and grain boundary migration). Thus VPSC simulations have been performed using both the tangent formulation (α= 1) and relaxed strain compatibility conditions (α = 10 and 100).

Qualitatively, all models predict a similar LPO evolution; with progressive strain, olivine [100] and [010] axes tend to concentrate close to the maximum stretching and shortening directions, respectively. Yet LPOs predicted by the two approaches do differ, even if, from a mechanical point of view, VPSC models with α = 100 and equilibrium-based simulations are very similar. The difference arises because the grain reorientation that results from the discrepancy between the deformations of the grain and of the surrounding medium (last term in the right-hand side of equation (4)) is not

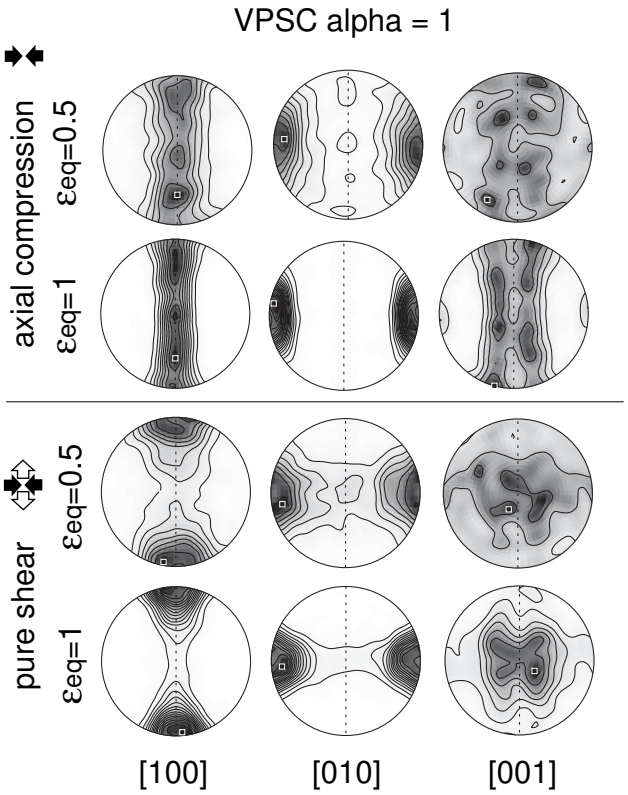

Figure 2. Olivine lattice preferred orientations developed in axial compression and pure shear at equivalent strains ε_{eq} of 0.5 and 1. Anisotropic VPSC model, α = 1, high-temperature critical resolved shear stresses (Table 2). Lower hemisphere equal-area projections are shown: 1000 grains, contours at 0.5 m.u.d. intervals. Inverse-log shading varies from white (minimum density) to black (maximum density, also indicated by a solid square). Dashed lines mark the foliation; lineation is horizontal.

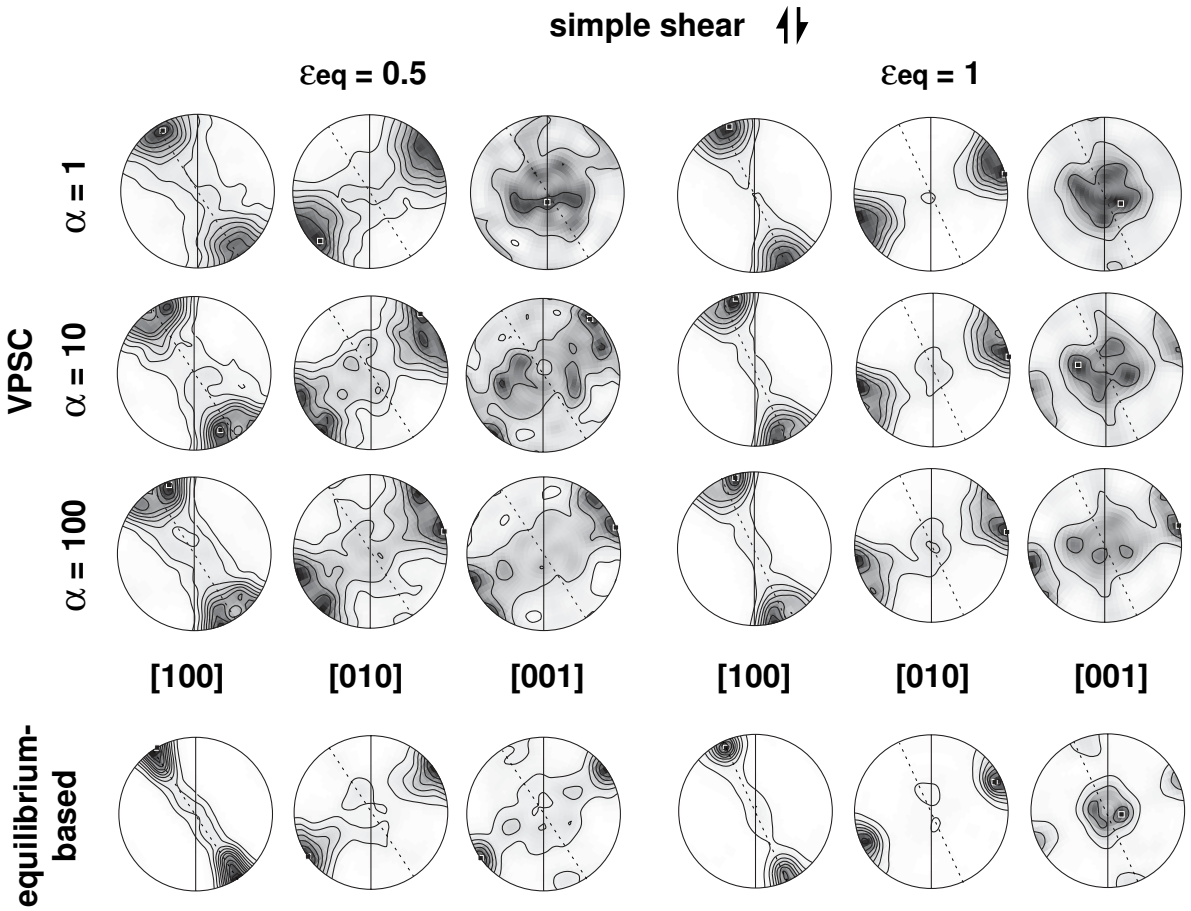

Figure 3. Olivine lattice preferred orientations developed in dextral simple shear at equivalent strains ε_{eq} of 0.5 and 1 in anisotropic VPSC models with α = 1, 10, and 100 and in the equilibrium-based model. Lower hemisphere equal-area projections are shown: 1000 grains, contours at 0.5 m.u.d. for ε_{eq}=0.5 and 1 m.u.d. for ε_{eq}=1. Inverse-log shading varies from white (minimum density) to black (maximum density, also indicated by a solid square). Solid lines mark the shear plane; shear direction is horizontal. Dashed lines mark the foliation; lineation is horizontal.

considered in equilibrium-based simulations. This term, null for spherical grains, increases rapidly as the grains become elongated. At an equivalent strain of 0.5, for instance, it is, on average, one half of the plastic spin. Indeed, VPSC models with α = 100 and no grain shape reorientation predict LPOs very similar to those obtained in equilibrium-based simulations.

In simple shear (Figure 3) equilibrium-based models predict that the LPO reorientation closely follows the finite strain ellipsoid rotation. On the other hand, in VPSC simulations the LPO evolves with progressive shearing from a bimodal pattern characterized by a weakly asymmetric distribution of [100] and [010] relative to the maximum *X* and minimum *Z* principal finite elongation directions to a single maxima pattern in which [100] is intermediate between the macroscopic shear and principal finite elongation directions and [010] is approximately normal to the shear plane. This LPO evolution is faster if strain compatibility is relaxed (α > 1, Figures 3 and 4). The [010] and [001] axes distribution is also modified (Figure 3). In models with α = 1 the LPO pattern tends toward an orthorhombic symmetry with [010] at high angle to the shear plane and [001] near the intermediate principal strain direction *Y*. In contrast, in models with α > 1, [010] and [001] tend to form girdles normal to the [100] concentration, i.e., at high angle to both the shear and the maximum finite elongation directions. Single maxima patterns are only approached at large finite strains.

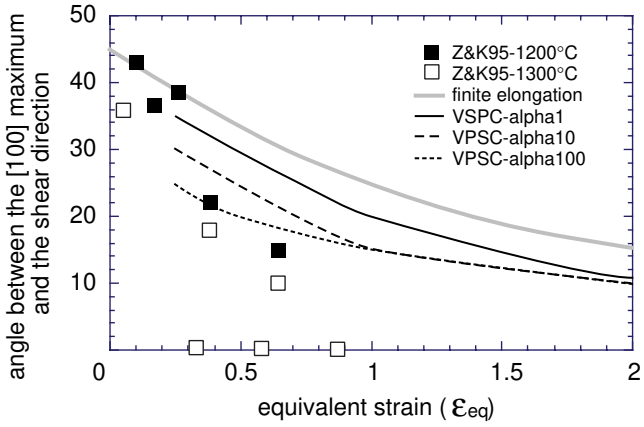

Figure 4. Evolution of the angle between the maximum density of olivine [100] axis and the shear direction with finite strain in anisotropic VPSC models with α = 1, 10, and 100 and in experimental simple shear deformation of olivine aggregates at 1200°C (solid squares) and 1300°C (open squares) [*Zhang and Karato,* 1995]. In equilibrium-based models, the [100] maximum evolves as the principal finite elongation direction (thick gray line).

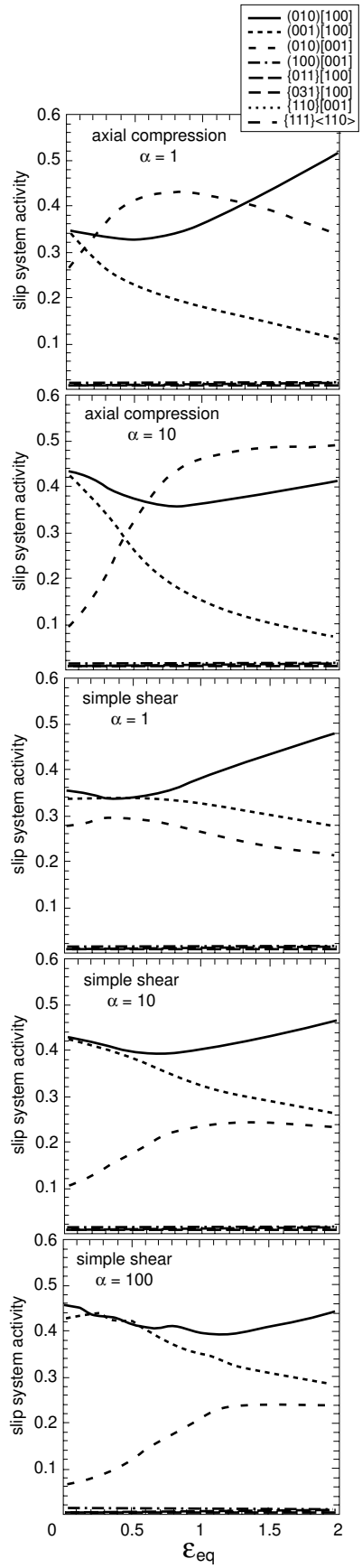

For instance, in simulations with $\alpha = 100$, at an equivalent strain of 2, [010] and [001] still form weak girdles at high angle to the shear plane.

LPO evolution is directly related to the slip system activity.

Figure 5. Evolution of the slip system activity with finite strain in axial compression and simple shear for VPSC models with different α values.

The relative activity of slip systems in VPSC simulations of axial compression and simple shear is displayed in Figure 5. Pure shear results are similar to simple shear ones and therefore not shown. In all models, the three main slip systems accommodate more than 95% of the deformation. Because of the more stringent geometrical constraints the activity of the "hard" (010)[001] system is higher in axial compression than in simple shear. Geometrical effects resulting from interactions between the three main slip systems may be observed in simple shear. Similar critical resolved shear stresses are ascribed to (010)[100] and (001)[100], and these two systems initially display equivalent activities. This leads to the development of a LPO pattern with a girdle distribution of both [010] and [001]. However, as deformation proceeds, strain compatibility constraints induce an increase of the (010)[001] activity. This is followed by an increase in (010)[100] activity and development of a single maxima LPO pattern characterized by a concentration of [010] and [100] axes normal to flow plane and close to the flow direction, respectively. Relaxation of strain compatibility constraints reduces the need for (or slows) significant slip on the “hard” (010)[001] system, allowing the subsistence of {0kl}[100] patterns at larger finite strains.

Since critical resolved shear stresses for olivine slip systems depend on a large number of physical parameters, such as temperature and stress (or strain rate), it is important to test the sensitivity of model predictions to the ascribed critical resolved shear stresses. In the previous models most of the deformation is accommodated by the three main olivine slip systems: (010)[100], (001)[100], and (010)[001] (Figure 5). One may infer that the critical resolved shear stresses of the remaining nonindependent slip systems do not affect model predictions as far as they are higher than those ascribed for the main ones.

In fact, modeled olivine LPO evolutions are insensitive to variations of the critical resolved shear stress values within the range of “reasonable” values for high-temperature deformation. For instance, a ten fold increase of the (010)[001] critical resolved shear stress has no effect on the predicted LPO. Figure 6 displays LPO orientations developed in a simple shear VPSC simulation with critical resolved shear stresses $\tau_0^{(010)[001]} = 2\tau_0^{(010)[100]} = 3\tau_0^{(001)[100]}$ derived from stress curves

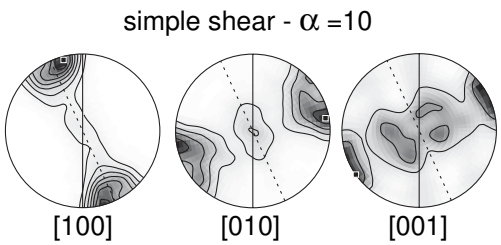

Figure 6. Olivine lattice preferred orientations developed at $\varepsilon_{eq} = 1$ in a dextral simple shear VPSC model with $\alpha = 10$ and $\tau_0^{(010)[001]} = 2\ \tau_0^{(010)[100]} = 3\ \tau_0^{(001)[100]}$. Lower hemisphere equal-area projections are shown: 1000 grains, contours at 1 m.u.d. intervals. Inverse-log shading varies from white (minimum density) to black (maximum density, also indicated by a solid square). Solid lines mark the shear plane; shear direction is horizontal. Dashed lines mark the foliation; lineation is horizontal.

for wet olivine single crystals [*Mackwell et al.*, 1985]. Although in this simulation the weakest slip system is (001)[100], the resulting LPO hardly differs from those of simple shear simulations in Figure 3. Distinct LPO patterns (Figure 7) are, however, obtained in models using critical resolved shear stresses inferred from low-temperature experiments (Table 3), in which slip on {hk0}[001] systems was dominant [*Phakey et al.*, 1972]. The [010] distribution remains similar to that observed in high-temperature simulations but [100] and [001] form crossed girdles slightly asymmetric relative to the *XY* plane. The [001] axis displays a weak maximum close to the shear direction. In addition, low-temperature simulations show a much slower LPO evolution.

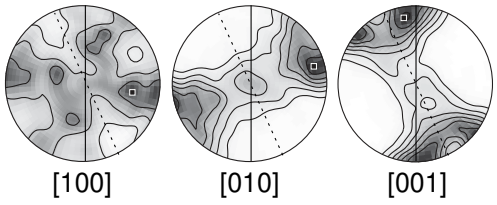

Figure 7. Olivine lattice preferred orientations developed at ε_{eq}=1 in a dextral simple shear VPSC model with α= 10 and low-temperature critical resolved shear stresses (Table 3). Lower hemisphere equal-area projections are shown: 1000 grains, contours at 0.5 m.u.d. intervals.. Inverse-log shading varies from white (minimum density) to black (maximum density, also indicated by a solid square). Solid lines mark the shear plane; shear direction is horizontal. Dashed lines mark the foliation; lineation is horizontal.

Table 3. Slip System Data Used to Simulate Low-Temperature Deformation

Slip System	Critical Resolved Shear Stress τ_0*	Stress Exponent *n*
(010)[100]	1	3.5
(001)[100]	0.5	3.5
(010)[001]	0.75	3.5
(100)[001]	0.5	3.5
{011}[100]	2	3.5
{031}[100]	2	3.5
{110}[001]	0.5	3.5
{111}[110]		
{111}[011]†	500	3.5

*Normalized relative to τ_0(010)[100].

†Since olivine displays only three independent slip systems, "complementary" pyramidal systems have to be used in the Taylor calculation of the initial solution (first iteration), but they are not used in the subsequent VPSC iterations.

In summary, equilibrium-based and VPSC simulations predict similar LPO evolutions in nonrotational deformations: Olivine crystallographic axes [100] and [010] tend to concentrate at low angle to the principal finite strain directions *X* and *Z*. On the other hand, in simple shear, whereas equilibrium-based models predict that olivine [100] and [010] axes will align in the *X* and *Z* directions, respectively, in VPSC models these maxima are displaced toward the shear direction and the normal to the shear plane, respectively. Once developed, these patterns remain stable and become more and more concentrated as the deformation proceeds (Figure 8). LPO evolution is faster in nonrotational deformation than in simple shear, and in both cases, LPO concentrates much faster in lower bound models.

Comparison with previous polycrystal plasticity models shows that for nonrotational deformation, predictions from different models largely agree. The main difference is a faster LPO development in equilibrium-based (*Chastel et al.* [1993] and this work) and constrained-hybrid models [*Parks and Ahzi*, 1990]. In simple shear, however, some slight, but significant, differences arise between the various models. Equilibrium-based and relaxed Taylor [*Takeshita*, 1989] models predict that the olivine LPO tends to align with the finite strain markers (lineation and foliation). In anisotropic VPSC simulations with α = 1, as in previous isotropic [*Takeshita et al.*, 1990] and "*n*-site" [*Wenk et al.*, 1991] self-consistent models, the [100] and [010] axes are not parallel but display a weakly asymmetric distribution relative to the maximum and minimum finite elongation directions. It is interesting to notice that anisotropic VPSC simulations with α = 1 closely reproduce the LPO evolution predicted in *n*-site VPSC models [*Wenk et al.*, 1991], which explicitly account for the nearest neighbor interactions but are significantly more time-consuming. Finally, anisotropic VPSC models with relaxed strain compatibility (α > 1) display a clearly asymmetric distribution of the [100] and [010] axes relative to the maximum and minimum finite elongation directions. In these models the LPO evolves with increasing strain from an asymmetric bimodal distribution of the [100] and [010] axes to a single maxima pattern characterized by [100] and [010] concentrations intermediate between the finite strain and the macroscopic shear directions. A bimodal distribution of the slip plane relative to the foliation is also observed in simulations by *Ribe and Yu* [1991] and in 2-D finite difference models [*Zhang et al.*, 1994], but the asymmetry is weaker. In sections 5 and 6, we will discuss these contrasting predictions in the light of LPO development during experimental deformation of olivine polycrystals as well as LPO data from naturally deformed peridotites.

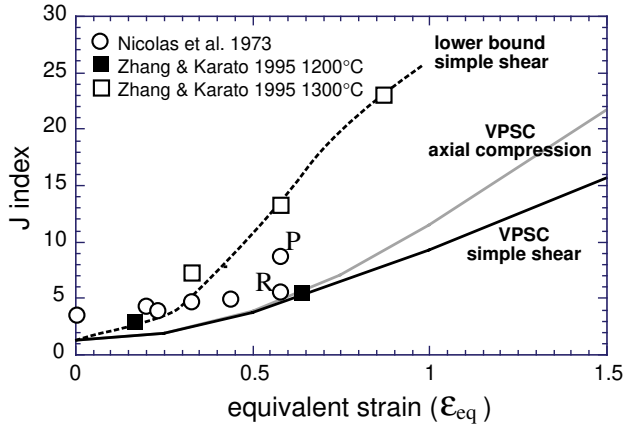

Figure 8. Evolution of LPO intensity (represented by the *J* index, i.e., the integral of the orientation distribution function [*Bunge*, 1982]) as a function of the equivalent strain in axial compression for anisotropic VPSC models (α = 1; solid gray line) and for *Nicolas et al.* [1973] experiments (open circles: P, porphyroclasts; R, recrystallized grains). Similar curves are shown for simple shear as predicted by lower bound (dashed line) and VPSC (α = 1; solid black line) models and observed by *Zhang and Karato* [1995] in experiments at 1200°C (solid squares) and 1300°C (open squares). VPSC models with relaxed strain compatibility conditions (not shown) display an evolution slightly faster than VPSC models with α = 1 but much slower than lower bound models.

5. Constraints From Experimental Data

Data on LPO evolution during experimental deformation of olivine polycrystals are limited to two sets of experiments: one in axial compression [*Nicolas et al.*, 1973] and one in simple shear [*Zhang and Karato*, 1995]. In both cases, synthetic olivine polycrystals were deformed under high-temperature (1200°-1300°C), high strain rate (~10^{-5} s^{-1}) conditions. LPO were also measured in the triaxial deformation experiments of *Avé-Lallemant and Carter* [1970] and *Kunze and Avé-Lallemant* [1981], but these measurements were done in highly recrystallized domains of the specimens. They cannot therefore be used to test the predictions of polycrystalline plasticity models that simulate LPO development by dislocation glide only. Yet comparison of LPO of strongly recrystallized samples with model predictions allows us to assess how recrystallization processes, omnipresent in the natural deformation of upper mantle rocks, modify the dislocation glide patterns.

5.1. Axial Compression

LPO evolution in axial compression experiments by *Nicolas et al.* [1973] is characterized by a progressive rotation of [010] toward the compression direction, while [100] and [001] tend to concentrate in a diffuse and a sharp girdle, respectively, normal to this direction (Figure 9). This pattern agrees, to a first approximation, with the one predicted by different polycrystalline plasticity models. However, simulated and measured LPO patterns differ by their relative organization of the [100] and [001] axes. In the simulations (Figure 2) the [100] axes form a sharp girdle, whereas the [001] axis distribution is more diffuse. The discrepancy between observed and modeled LPO may be explained by activation of different slip systems. In the experiments, slip on {hk0}[001] systems probably played a significant role in the deformation (activity of the {110}[001] system was inferred from the study of deformed bubbles), while the microscopic parameters used in the models (Table 2) induce dominant activity of {0kl}[100] systems. Activation of low-temperature slip systems at temperatures of 1200°-1300°C is probably due to the high stresses (1.3-1.5 GPa) involved in the experiments. Indeed, simulations using low-temperature microscopic parameters (Table 3) better reproduce the experimental LPO pattern (Figure 10), but the activation of a large number of slip systems leads to a slower LPO evolution in "low-temperature" simulations.

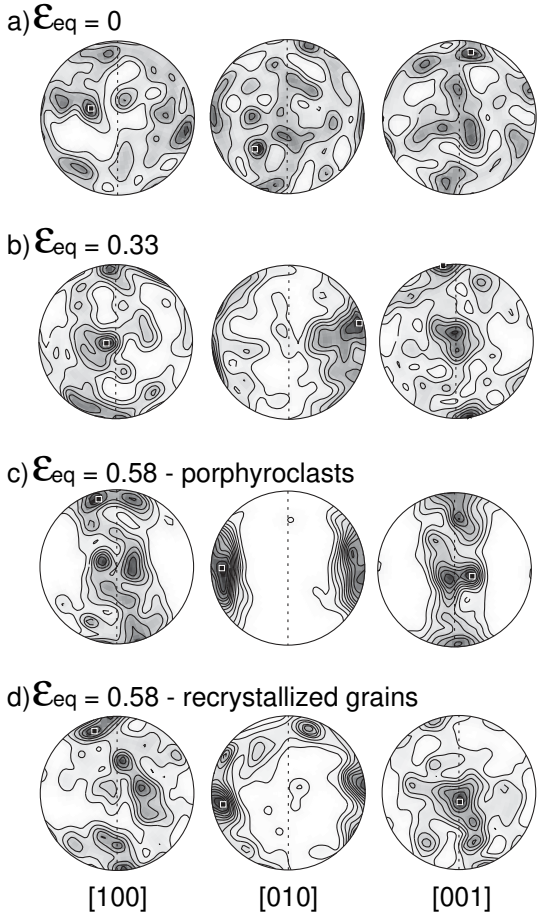

Figure 9. Olivine lattice preferred orientations developed in dunites submitted to axial compression under high-temperature, high-pressure experimental conditions [*Nicolas et al.,* 1973]. (a) Starting material. (b) Equivalent strain ε_{eq} = 0.33. (c) ε_{eq} = 0.58 (porphyroclasts). (d) ε_{eq} = 0.58 (neoblasts). Lower hemisphere equal-area projections are shown: contours at 0.5 m.u.d. intervals. Inverse-log shading varies from white (minimum density) to black (maximum density, also indicated by a solid square). Dashed lines mark the foliation (normal to the compression σ_1).

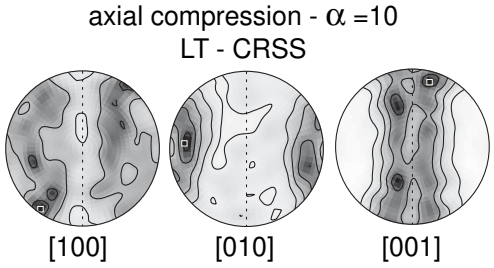

Figure 10. Olivine lattice preferred orientations developed at an equivalent strain ε_{eq} of 0.5 in an axial compression VPSC model with α = 10 and low-temperature critical resolved shear stresses (Table 3). Lower hemisphere equal area projections are shown: 1000 grains, contours at 0.5 m.u.d. intervals. Inverse-log shading varies from white (minimum density) to black (maximum density, also indicated by a solid square). Dashed lines mark the foliation (normal to the compression direction σ_1).

At similar finite strains, experimental samples show LPO intermediate between those predicted in high-temperature anisotropic VPSC and equilibrium-based simulations (Figure 8). A direct comparison is nevertheless difficult, since the experimental samples displayed a nonrandom, initial LPO (the *J* index of the undeformed sample is 3.43). In addition, dynamic recrystallization by nucleation of new grains within highly strained domains of the specimens (50% of the sample is recrystallized at 0.58 equivalent strain) affects LPO intensity. Recrystallized grains and porphyroclasts display similar LPO patterns, but while porphyroclasts show a much stronger LPO than predicted in our VPSC simulations, recrystallized grains display a weaker LPO. This suggests that nucleation recrystallization during coaxial deformation under high-stress deformation conditions has a double effect on LPO intensity. Recrystallized grains display a clear misorientation relative to the parent grains; the LPO is weakened. On the other hand, grains in hard orientations (e.g., those with [100] parallel to

$\sigma 1$) suffer intense kinking [*Nicolas et al*., 1973] and act therefore as preferential sites for recrystallization. Selective recrystallization of grains in hard orientations may help to concentrate the LPO. Fast LPO development associated with dynamic recrystallization is also observed in triaxial compression experiments ($\sigma 1 > \sigma 2 > \sigma 3$) under wet conditions [*Avé-Lallemant*, 1975]. In these tests, intense dynamic recrystallization occurred, and a strong LPO develops at lower strains than in the experiments of *Nicolas et al.* [1973].

From these observations we suggest that LPO development in an olivine polycrystal submitted to axial compression may be predicted using the anisotropic VPSC approach. Equilibrium-based models predict the correct patterns, but the LPO concentrates too rapidly. Although a better fit to the LPO developed in the experiments of *Nicolas et al.* [1973] is obtained using microscopic parameters derived from single crystal deformation under low temperature conditions, under natural strain rates the transition between the low- and high-temperature behavior should occur at much lower temperatures. Indeed, few naturally deformed peridotites display LPO patterns with an axial [010] symmetry (Figure 1), but these rocks show, systematically, a stronger concentration of [100] than of [001]. Finally, dynamic recrystallization probably does not modify the typical axial compression LPO pattern but rather contributes to an initially faster development and stabilization of this LPO.

5.2. Simple Shear

LPO developed in fine-grained synthetic olivine aggregates submitted to simple shear in a gas medium apparatus at temperatures of 1200°C and 1300°C [*Zhang and Karato*, 1995; S. *Zhang et al.*, Simple shear deformation of olivine aggregates, submitted to Tectonophysics, 1999 (hereinafter referred to as Zhang et al., submitted manuscript, 1999)] are displayed in Figure 11. Samples deformed to shear strains $\gamma > 0.5$ show clear evidence of dynamic recrystallization due to both subgrain rotation and grain boundary migration, the degree of recrystallization being significantly higher in samples deformed at 1300°C (>80% for a specimen deformed to $\gamma = 1.5$ [*Zhang and Karato*, 1995]). Thus simulation predictions should be tested against the 1200°C data. In addition, comparison between LPOs formed at 1200°C and 1300°C should allow us to evaluate the effect of dynamic recrystallization on LPO.

LPO formed in simple shear at 1200°C (Figure 11a) exhibits a statistically orthorhombic pattern, which results from dominant slip on (010)[100] [*Zhang and Karato*, 1995]. This first-order pattern is in agreement with the predictions of all polycrystal plasticity models. A finer observation shows that [100] displays a bimodal distribution whose peak is intermediate between the shear direction and the maximum finite elongation direction *X*. The best fit to this asymmetric pattern is obtained for anisotropic VPSC models with relaxed strain compatibility ($\alpha > 1$). Moreover, although a direct comparison is hindered by the fact that the experimental samples probably displayed a nonrandom initial LPO, LPO intensities for samples submitted to a shear strain γ of 1.1 are similar. Yet slight differences between model predictions and observations exist. In particular, experimental samples display a stronger concentration of [001] within the shear plane than the one predicted by anisotropic VPSC models. This may result from a lower activity of the (001)[100] and (010)[001] systems in the experiments.

In order to evaluate if the differences between model and experiment are not due to a small amount of shortening normal to the shear plane in the experiments, we compared VSPC predictions for transpression [*Tommasi et al.*, 1999] to the experimental data. LPO patterns developed in plane transpression are similar to those predicted for simple shear, but the reorientation of the main [100] maximum toward the shear direction is faster than the one observed in the 1200°C experiments. This suggests that although changes in the thickness of the samples indicate a small amount of shortening normal to the shear plane [*Zhang and Karato*, 1995; Zhang et al., submitted manuscript, 1999], simple shear was dominant in the experiments.

Samples deformed at 1300°C display a LPO pattern characterized by a faster reorientation of the [100] and [010] maxima into parallelism with the flow direction and the normal to the shear

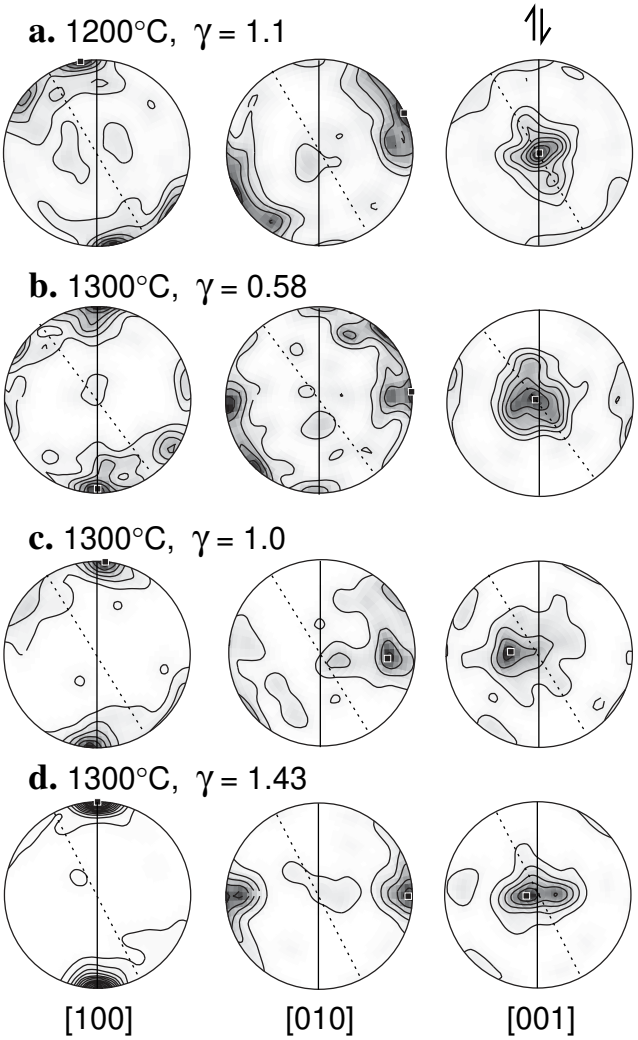

Figure 11. Olivine lattice preferred orientations developed in dunites submitted to dextral simple shear under high-temperature, high-pressure experimental conditions [*Zhang and Karato*, 1995; S. Zhang, personal communication, 1997]: (a) 1200°C, $\gamma = 1.1$ (ε_{eq}= 0.64); (b) 1300°C, $\gamma = 0.58$ (ε_{eq}= 0.33); (c) 1300°C, $\gamma = 1.0$ (ε_{eq}= 0.58); (d) 1300°C, wet, $\gamma = 1.43$ (ε_{eq}= 0.83). Lower hemisphere equal-area projections are shown: contours at 1 m.u.d. intervals in Figures 11a and 11b and 2 m.u.d. intervals in Figures 11c and 11d. Lowest contour is 1 m.u.d. in all cases. Inverse-log shading varies from white (minimum density) to black (maximum density, indicated by a solid square). Solid lines mark the shear plane; shear direction is horizontal. Dashed lines mark the foliation; lineation is horizontal.

plane, respectively (Figures 11b, 11c, and 11d). This suggests that in simple shear dynamic recrystallization processes (in the experiments, mainly subgrain rotation [*Zhang and Karato*, 1995]) do not merely affect LPO intensity (LPO development is faster, Figure 8) but modify the pattern. A similar evolution was observed in simple shear deformation of ice [*Bouchez and Duval*, 1982] and calcite [*Schmid et al.*, 1987] at high homologous temperatures. Experimentally sheared ice polycrystals, in particular, display a clear evolution from a LPO characterized by bimodal distribution of the main slip plane (0001) relative to the foliation to a single maximum pattern in which (0001) is aligned with the shear plane [*Bouchez and Duval*, 1982]. These observations suggest that during simple shear, recrystallization by either subgrain rotation or grain boundary migration leads to a single maxima LPO in which the main slip system parallels the macroscopic shear.

In summary, although all polycrystal plasticity models reproduce the gross characteristics of LPO evolution in simple shear, the best fit to the asymmetric bimodal LPO patterns observed in simple shear experiments at 1200°C is obtained using anisotropic VPSC simulations with relaxed strain compatibility. Dynamic recrystallization will induce a faster reorientation of LPO, resulting in a single maxima LPO characterized by parallelism between (010)[100] and the macroscopic shear. Yet at a shear strain of 1 the angular misorientation between modeled and measured LPO is <15° if anisotropic VPSC models with relaxed strain compatibility (α = 10 or 100) are used. Thus we suggest that these simulations bear reasonable first-order predictions of LPO development during simple shear deformation in the upper mantle.

6. Constraints From Naturally Deformed Peridotites

Analysis of the olivine LPO database (more than 120 naturally deformed peridotites) compiled in the Laboratoire de Tectonophysique de l'Université de Montpellier II, France [*Ben Ismail and Mainprice*, 1998] allows some further constraints to be put on model predictions, particularly on those for simple shear, since most samples are from ophiolites and record therefore flow in the vicinity of mid-ocean ridges; an environment in which large homogeneous deformation in a regime close to simple shear is the most common situation [*Nicolas*, 1989, p. 27]. Predominance of simple shear or combinations of simple and pure shear in nature is also suggested by the comparison between the database and LPO patterns predicted for different strain regimes [*Tommasi et al.*, 1999].

6.1. LPO Patterns

Indeed, there is a good first-order agreement between model predictions in simple shear and LPO patterns observed in naturally deformed peridotites. With exception of a few samples, naturally deformed peridotites essentially display two LPO patterns (Figure 1), which are associated with slip on (010)[100] or on several of the {0kl}[100] systems, in particular, (010)[100] and (001)[100]. This is in agreement with single-crystal deformation data that suggest that although the (010)[100] system is the weakest under a wide range of upper mantle deformation conditions, strengths of (010)[100] and (001)[100] are often similar and (001)[100] may even be weaker at low-temperature and low oxygen fugacity or wet deformation conditions [*Bai et al*., 1991; *Mackwell et al.*, 1985]. Another common feature of both naturally deformed peridotites and modeled LPO is a slight dispersion of both [100] and [001] within the foliation that may be interpreted as resulting from secondary slip on (010)[001].

Dominant simple shear deformation is also suggested by the general asymmetry of the LPO relative to the finite strain markers (lineation and foliation) in naturally deformed peridotites. A symmetric distribution of [100] relative to the lineation is observed in <10% of the samples. The angle between the [100] maximum and the lineation is, however, highly variable, ranging from 0° to 35°. These angle measurements probably contain significant errors, since, in many samples, the weak grain shape fabric hinders a precise determination of the structural reference frame. Nevertheless, the systematic asymmetry of the natural LPO suggests that anisotropic VPSC models better reproduce LPO development in simple shear than lower bound and relaxed Taylor models.

Although less common, LPO patterns similar to those produced in axial compression simulations are observed in some peridotitic xenoliths from cratonic environments and, more rarely, in ophiolitic peridotites or lherzolitic massifs. These patterns are characterized by a well-developed [010] maximum normal to the foliation and [100] and [001] in girdles in the foliation plane. However, different from the LPO developed during the axial compression experiments of *Nicolas et al*. [1973], axial [010] patterns developed in peridotitic xenoliths are characterized by sharp [100] and diffuse [001] girdles. They are therefore reproduced in axial compression polycrystal plasticity simulations using high-temperature CRSS.

On the other hand, a few samples display LPO patterns that cannot be produced in numerical simulations. For instance, dunites from the southern ophiolite massifs in New Caledonia deformed under high-temperature conditions often display strong orthorhombic LPO patterns with [001] normal to the foliation (Figure 1) that suggest dominant activity of (001)[100] [*Cassard*, 1980]. Similar LPO patterns are also observed in porphyroclastic peridotites in the Betic Cordillera [*Garcia-San Millan*, 1998] and in the Erro-Tobbio massif in the Alps [*Van der Wal*, 1993]. Indeed, single crystal deformation experiments indicate that under wet conditions, (001)[100] is the weakest system [*Mackwell et al.*, 1985]. However, simulations using the critical resolved shear stresses predicted by these experiments fail to reproduce this LPO pattern (Figure 6). As deformation proceeds, increasing activity on (010)[001] (due to strain compatibility constraints) produces a reorientation of the grains that results in dominant activity of (010)[100], even if the lowest critical resolved shear stress is ascribed to (001)[100]. This suggests that (001)[100] LPO patterns may only develop if (010)[001] is not activated. In nature this may have been possible because the deformation was partially accom-

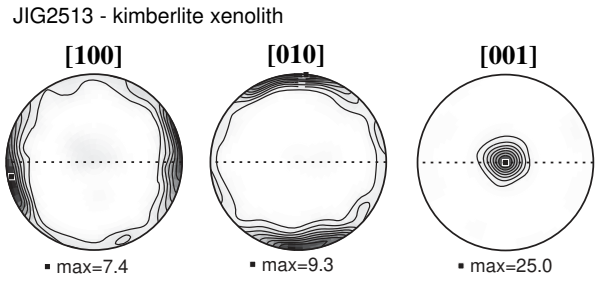

Figure 12. Olivine LPO in a kimberlite xenolith from the Kaapval craton. Lower hemisphere equal-area projections are shown: contours at 1 m.u.d. intervals, except for [001], which is contoured at 3 m.u.d. intervals. Inverse-log shading varies from white (minimum density) to black (maximum density, also indicated by a solid square). Dashed lines mark the foliation; lineation is horizontal.

modated by dynamic recrystallization by subgrain rotation and/or grain boundary migration [*Cassard*, 1980; *Garcia-San Millan*, 1998]. Finally, some peridotitic xenoliths from the Kapvaal craton [*Mainprice et al.*, 1997] and peridotites from the Alpe Arami massif [*Bascou*, 1998; *Mockel*, 1969] display anomalous axial [001] LPO patterns (Figure 12) that cannot be formed by dislocation glide on known olivine slip systems.

Comparison between LPO evolution in models and LPO patterns of naturally deformed upper mantle rocks may also carry some information on the deformation mechanisms active during natural deformation. The {0kl}[100] patterns (Figure 1) represent at least half of the natural patterns. Yet, in simulations, LPO patterns typical of slip on several of the {0kl}[100] slip systems are only produced in VPSC models with relaxed strain compatibility, in which the "hard" (010)[001] system displays a low activity (Figure 5). This suggests that in nature, olivine may deform without significant slip on (010)[001] provided that other deformation mechanisms, like dynamic recrystallization or grain boundary sliding, accommodate strain incompatibility. Indeed, *Zhang and Karato* [1995] note that significant contribution of dislocations with **b** = [001] to deformation is restricted to samples deformed at 1200°C, which display a less effective dynamic recrystallization.

6.2. LPO Evolution With Finite Strain

In the models, LPO intensity evolves continuously with strain. For shear strains ≥3, VPSC models predict extremely concentrated LPO ($J \geq 20$, Figure 8). Naturally deformed peridotites, on the other hand, seldom display very strong LPO. Their J indexes cluster between 4 and 14 (Figure 13), suggesting that for most natural samples the LPO records shear strains apparently <3 (Figure 8). Yet many samples come from the shallow upper mantle of fast oceanic ridges, where large shear strains are expected to occur [*Nicolas*, 1989].

A possible explanation is that dynamic recrystallization by subgrain rotation, which is not simulated in the models, stabilizes the LPO. Subgrain rotation is characterized by subdivision of strained porphyroclasts into new grains displaying a misorientation >15° relative to the parent grain [*Poirier and Nicolas*, 1975]. This may induce a progressive diffusion of LPO that will counterbalance the LPO intensification due to dislocation glide, giving rise to a stable LPO. Scatter in LPO due to subgrain rotation recrystallization has been documented in naturally deformed peridotites (Figure 14)

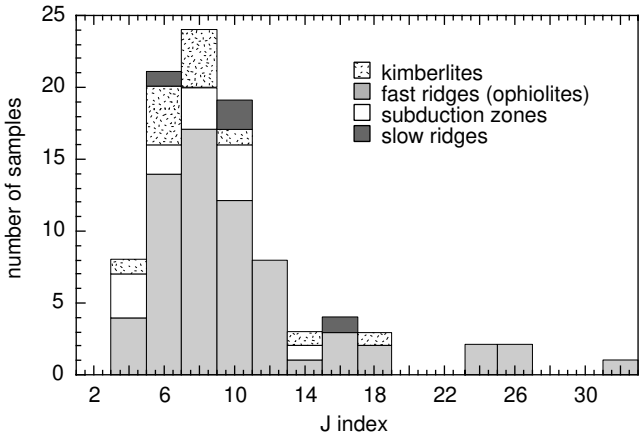

Figure 13. LPO intensity (J index) in naturally deformed peridotites (data from *Ben Ismail* [1995]).

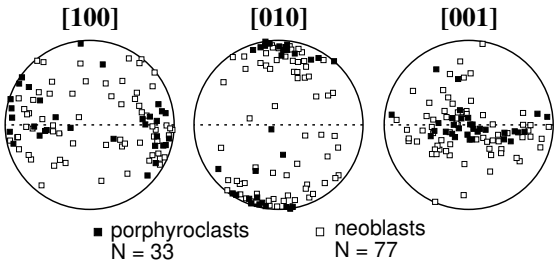

Figure 14. Olivine LPO in a porphyroclastic peridotite xenolith from Eglazine, Massif Central, France [R. Hoffmann, personal communication, 1998]. Lower hemisphere equal-area projections are shown. Solid squares, porphyroclasts; open squares, neoblasts. Dashed lines mark the foliation; lineation is horizontal.

and quartzites [*Law*, 1986; *Lloyd and Freeman*, 1994] and in recrystallization experiments on olivine single crystals [*Karato*, 1988; *Toriumi and Karato*, 1985]. For olivine, dominant slip on (010)[100] leads to development of (100) tilt boundaries. If recrystallization takes place by progressive misorientation along these boundaries, the rotation axis should be [001] [*Poirier and Nicolas*, 1975]. This process will induce a dispersion of both [100] and [010] in the *XZ* plane (normal to the foliation and parallel to the lineation) often observed in naturally deformed peridotites (Figure 1, (010)[100] pattern) but not reproduced in our models (Figure 3).

Under low-temperature, high-deviatoric stress deformation conditions, dynamic recrystallization by nucleation and growth of strain-free neoblasts at grain boundaries [*Drury et al.*, 1991] may also result in an effective weakening of the LPO [*Boudier and Coleman*, 1981; *Nicolas et al.*, 1973]. In addition, the resulting fine-grained texture may favor the activation of grain boundary sliding, which may partially or completely erase a previously developed high-temperature LPO [*Boullier and Gueguen*, 1975; *Jaroslow et al.*, 1996].

7. Prediction of Upper Mantle Seismic Anisotropy

If single crystal elastic stiffness coefficients, the volume fraction of the different mineral phases composing an aggregate, and their crystallographic preferred orientation are known, the elastic properties of the aggregate may be calculated using a Voigt-Reuss-Hill average of the stiffnesses (C_{ijkl}) over all crystal orientations [*Mainprice*, 1990]. Seismic properties calculated for olivine LPO modeled using the anisotropic VPSC agree qualitatively with those calculated using the measured LPO of a naturally deformed upper mantle rock with similar LPO intensity (Figure 15). Angular misorientations between seismic properties calculated for model and natural aggregates decrease with increasing strain and are usually <15°. Moreover, the overestimation of LPO intensity in equilibrium-based models or in VPSC simulations at high strains does not affect seismic anisotropy estimates, because seismic anisotropy for both P and S waves does not display a linear dependence on LPO intensity or strain but tends to limiting values at high shear strains (Figure 16). Equilibrium-based models may, however, significantly overestimate the seismic anisotropy at low strains ($\varepsilon_{eq} < 1$).

The comparison between seismic properties calculated for a model aggregate (100% olivine) and a naturally deformed peridotite with a typical upper mantle composition (70% olivine, 30% enstatite) also highlights the effect of other mineral phases on the

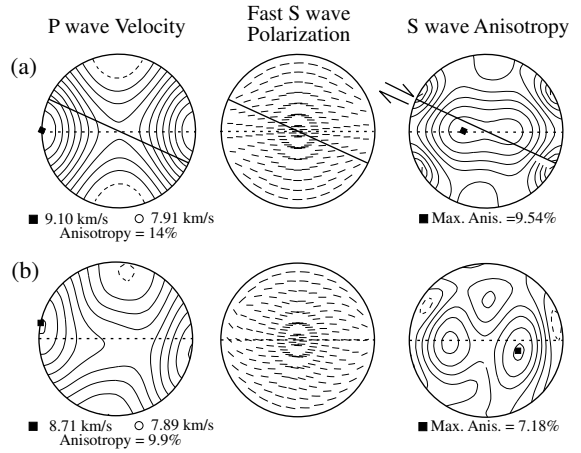

Figure 15. Calculated seismic properties (P wave velocity, fast S wave polarization plane, and S wave anisotropy) for (a) a model aggregate submitted to simple shear (100% olivine, VPSC model $\alpha = 10$, high-temperature CRSS, $\dot{\varepsilon}_{eq} = 1$, $J = 7.76$) and (b) a naturally deformed peridotite from the Oman ophiolite (sample 84OG61, 70% olivine, 30% enstatite, olivine LPO displayed in Figure 1, $J = 12.24$). Lower hemisphere equal-area projections are shown. Solid lines mark the shear plane; shear direction is horizontal. Dashed lines mark the foliation; lineation is horizontal. Solid squares indicate maximum values. P wave velocity and S wave anisotropy plots have 0.2 km/s and 1% contour intervals, respectively.

anisotropy (Figure 15). In spite of the stronger olivine LPO of the natural peridotite ($J = 12.24$) the model aggregate shows a much higher anisotropy for both P and S waves. The presence of enstatite leads to a dilution of the peridotite seismic anisotropy [*Mainprice and Silver*, 1993]. Thus model aggregates composed of olivine and enstatite would yield better predictions of upper mantle seismic anisotropy. Yet VPSC simulations of LPO development in enstatite-bearing aggregates are limited to low strains ($\varepsilon_{eq} \sim 0.5$) because of the high plastic anisotropy of enstatite crystals [*Wenk et al.*, 1991]. A way to circumvent this problem is to use in the seismic calculations an average orthopyroxene LPO obtained from measurements in naturally deformed peridotites. Enstatite deforms essentially on a single slip system (100)[001] [*Mackwell*, 1991]. Both LPO measurements in natural rocks as well as VPSC simulations of LPO development in olivine-enstatite aggregates [*Wenk et al.*, 1991] show a good correlation between the enstatite and olivine LPOs. We may therefore orient the average orthopyroxene LPO relative to the olivine LPO: The main slip direction and normal to the slip plane of enstatite, [001] and [100], are placed parallel to the olivine [100] and [010] axes, respectively.

Most previous numerical studies of olivine LPO and, hence, of seismic anisotropy development in the upper mantle used the equilibrium-based model [*Blackman et al.*, 1996; *Chastel et al.*, 1993]. We have seen that this model overestimates LPO intensities relative to both experimental data and the VPSC model (Figure 8). In addition, in simple shear, it predicts a [100] maximum parallel to the finite elongation direction (Figure 3), instead of at low angle to the shear direction. Yet seismic properties estimated using the equilibrium-based and the anisotropic VPSC models are very similar (Figure 17). This may be explained by: (1) the non linearity of the relationship between seismic anisotropy and LPO intensity: Overestimation of LPO intensity in equilibrium-based calculations only leads to overestimation of the seismic anisotropy for

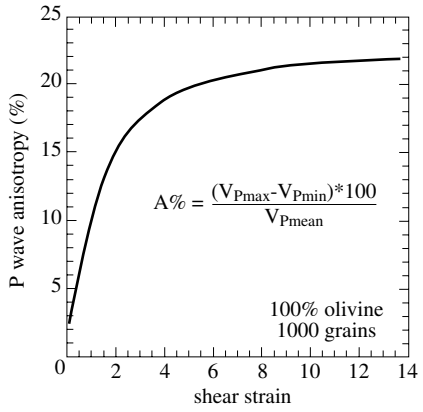

Figure 16. Calculated P wave anisotropy (A%) as a function of strain for a model aggregate submitted to simple shear (VPSC model, $\alpha = 10$, high-temperature critical resolved shear stresses). V_P is the P wave velocity.

weak deformations ($\varepsilon_{eq} < 1$); (2) the weak sensitivity of the seismic properties to details of the LPO. The elastic constants tensor is a fourth-order tensor, therefore the polycrystalline tensor is fully defined using the fourth-order harmonics of the ODF, while the complete LPO needs a much higher order description [*Bunge*, 1982; *Lapierre et al.*, 1996].

Thus, although equilibrium-based models are less accurate than VPSC simulations in the reproduction of LPO measured in naturally deformed and experimentally sheared peridotites, both models yield similar predictions of the development of upper mantle seismic anisotropy in response to plastic flow. Use of equilibrium-based models results in significant saving of computation time, which is particularly important when the LPO simulation is coupled to large-scale flow models.

8. Conclusion

Both stress-equilibrium and VPSC simulations of LPO development by dislocation glide under high-temperature conditions in olivine polycrystals show that in nonrotational deformation, olivine crystallographic axes [100] and [010] tend to concentrate at low angle to the principal finite strain directions *X* and *Z*. On the other hand, whereas equilibrium-based models predict similar orientations in simple shear, in VPSC models these maxima are displaced toward the shear direction and the normal to the shear plane, respectively. Both LPO result from slip on (010)[100] and, subsidiarily, on (001)[100] and (010)[001] systems. Once developed, these patterns remain stable and become more and more concentrated as the deformation proceeds. Analysis of these model results in the light of LPO data for experimentally and naturally deformed peridotites suggests that anisotropic VPSC models with relaxed strain compatibility bear finer predictions of LPO development during upper mantle flow.

Some of the characteristics of olivine LPO in naturally deformed peridotites are, nevertheless, not reproduced in any polycrystal plasticity model:

1. Whilst in the models, LPO evolves continuously with increasing strain and becomes very concentrated for axial strain >1 or shear strain >2, naturally deformed peridotites seldom display very strong LPO. This suggests that during natural deformation, other deformation mechanisms, in particular dynamic recrystallization by subgrain rotation or nucleation, counteract texture intensification due to dislocation glide, leading to a stable LPO. Thus

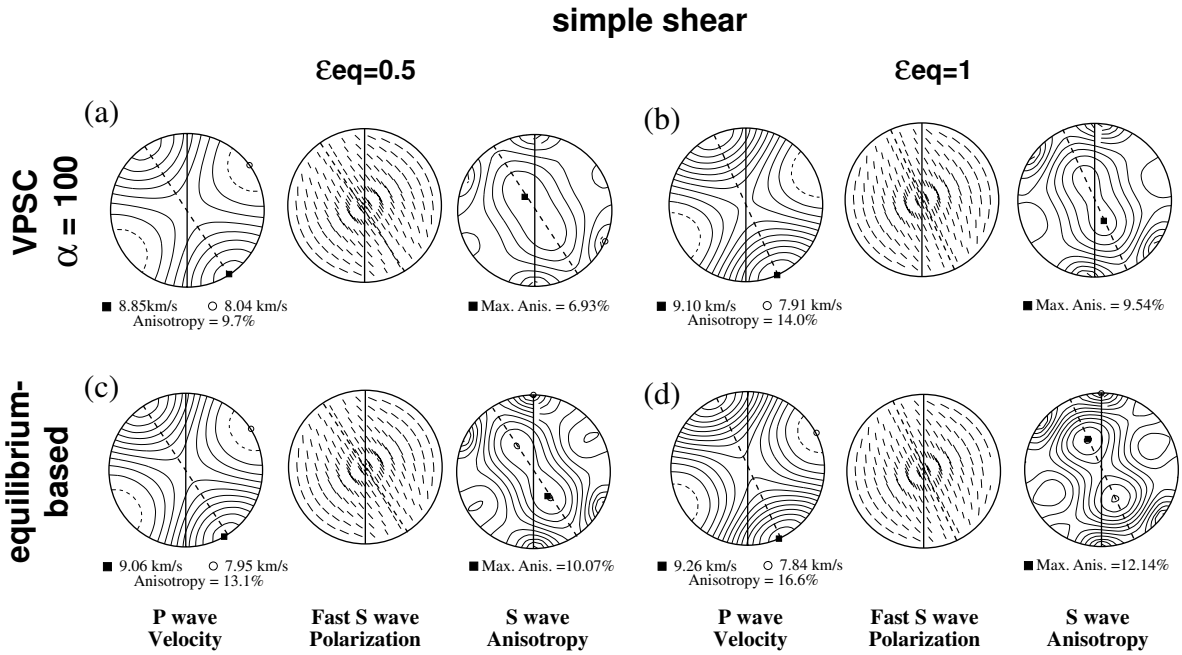

Figure 17. Seismic properties (P wave velocity, fast S wave polarization plane, and S wave anisotropy) calculated using LPOs predicted to develop in simple shear by (a and b) the anisotropic VPSC model with α=100 and (c and d) the equilibrium-based model after equivalent strains of 0.5 (Figures 17a and 17c) and 1 (Figures 17b and 17d). S wave anisotropy AV_S is defined as $AV_S = 2(V_{Smax}-V_{Smin})/(V_{Smax}+V_{Smin})$. Lower hemisphere equal-area projections are shown. Dashed lines mark the foliation; lineation is horizontal. Solid squares indicate maximum values. P wave velocity and S wave anisotropy plots have 0.1 km/s and 1% contour intervals, respectively. LPOs predicted by both models are presented in Figure 3.

the LPO intensity may only be used to infer the minimum amount of strain accommodated by a naturally deformed peridotite.

2. Experimentally sheared dunites at 1300°C show a faster LPO development associated with activation of dynamic recrystallization. At shear strains >0.5 a single maxima LPO characterized by parallelism between the main slip system (010)[100] with the macroscopic shear plane and direction is already developed. Most naturally deformed peridotites, which almost invariably suffered dynamic recrystallization, also display LPO patterns characterized by a single [100] maximum oblique to the lineation direction (*X* direction). Such patterns are not reproduced in equilibrium-based models and are only approached in anisotropic models after very high shear strains.

3. Finally, a few naturally deformed peridotites display (001)[100] or axial [001] LPO patterns that may not be reproduced in numerical simulations using the usual olivine slip systems, suggesting that they result from activation of other deformation mechanisms or static recrystallization. These abnormal LPO represent a small percent of the measured natural LPO, but one may wonder if the present sampling is representative of their abundance in the Earth's upper mantle.

Yet seismic properties calculated using LPO predicted by both anisotropic VPSC and equilibrium-based models closely reproduce those of most naturally deformed dunites. Both approaches yield good predictions of development of upper mantle seismic anisotropy in response to plastic flow. For simple shear, angular misorientation decreases with increasing strain and are usually <15°. Overestimation of LPO intensity in equilibrium-based models and in VPSC simulations at high strains does not affect seismic properties predictions, because these latter are weakly dependent on LPO intensity once a distinct LPO pattern has been developed. On the other hand, the diluting effect of other mineral phases, in particular orthopyroxene, has to be considered when predicting the upper mantle seismic anisotropy, if this latter is not to be overestimated.

Thus, although equilibrium-based models produce LPOs that differ significantly from those measured in naturally deformed and experimentally sheared peridotites, they may be used to predict the seismic properties produced by a given upper mantle deformation. Although it may overestimate the seismic anisotropy associated with weak deformations, this approach has the advantage of allowing the simulation of LPO development in olivine-enstatite polycrystals (i.e., typical upper mantle compositions) up to high strains. Moreover, its use results in a significant decrease in computation time, allowing fully coupled models of upper mantle deformation and LPO evolution.

Acknowledgments. A. Vauchez and O. Castelnau are thanked for numerous stimulating discussions throughout the evolution of this project. A. Nicolas and F. Boudier shared with us some of their considerable experience on the deformation of peridotites. We are indebted to S. Zhang for providing unpublished LPO data from simple shear experiments and to R. Lebensohn for making the VPSC code available. During part of this work, A.T. was a postdoctoral fellow at the University of Leeds, U.K., funded by the Marie Curie European Economic Community Scholarship ERBC4001GT961583.

References

Avé-Lallemant, H.G., Structural and petrofabric analysis of an "alpine-type" peridotite: The lherzolite of the french Pyrenees, *Leidse Geol. Meded.*, *42*, 1-57, 1967.

Avé-Lallemant, H.G., Mechanisms of preferred orientations in olivine in tectonite peridotites, *Geology*, *3*, 653-656, 1975.

Avé-Lallemant, H.G., and N.L. Carter, Syntectonic recrystallization of olivine and modes of flow in the upper mantle, *Geol. Soc. Am. Bull.*, *81*, 2003-2020, 1970.

Babuska, V., Elasticity and anisotropy of dunite and bronzitite, *J. Geophys. Res*, *77*, 6955-6965, 1972.

Bai, Q., and D.L. Kohlstedt, High-temperature creep of olivine single crystals, 2, Dislocation structures, *Tectonophysics*, *206*, 1-29, 1992.

Bai, Q., S.J. Mackwell, and D.L. Kohlstedt, High-temperature creep of

olivine single crystals, 1, Mechanical results for buffered samples, *J. Geophys. Res.*, *96*, 2441-2463, 1991.

Bascou, J., Etude pétrophysique des roches de haute pression du manteau et de la croûte éclogitique: exemple du Massif de Alpe Arami, Diplôme d'Etudes Approfondis, Univ. Montpellier II, Montpellier, France, 1998.

Ben Ismail, W., Variation de l'anisotropie sismique du manteau supérieur par l'étude de petrofabriques d'olivine, Diplôme d'Etudes Approfondis, Univ. Montpellier II, Montpellier, France, 1995.

Ben Ismail, W., and D. Mainprice, An olivine fabric database: An overview of upper mantle fabrics and seismic anisotropy, *Tectonophysics*, *296*, 145-158, 1998.

Blackman, D.K., and J.-M. Kendall, Sensitivity of teleseismic body waves to mineral texture and melt in the mantle beneath a mid-ocean ridge, *Philos. Trans. R. Soc. London*, *Ser. A, 355*, 217-231, 1997.

Blackman, D.K., J.-M. Kendall, P.R. Dawson, H.-R. Wenk, D. Boyce, and J. Phipps-Morgan, Teleseismic imaging of subaxial flow at mid-ocean ridges: Travel-time effects of anisotropic mineral texture in the mantle, *Geophys. J. Int.*, *127*, 415-426, 1996.

Bouchez, J.-L., and P. Duval, The fabric of polycrystalline ice deformed in simple shear: Experiments in torsion, natural deformation and geometrical interpretation, *Textures Microstruct.*, *5*, 1-17, 1982.

Boudier, F., and R.G. Coleman, Cross section through the peridotites in the Samail ophiolite, southeastern Oman mountains, *J. Geophys. Res.*, *86*, 2573-2592, 1981.

Boullier, A.M., and Y. Gueguen, S-P mylonites: Origin of some mylonites by superplastic flow, *Contrib. Mineral. Petrol.*, *50*, 121-134, 1975.

Boullier, A.M., and A. Nicolas, Classification of textures and fabrics of peridotites xenoliths from South African kimberlites, *Phys. Chem. Earth*, *9*, 467-475, 1975.

Bunge, H.J., *Texture Analysis in Materials Sciences*, 593 pp., Butterworths, London, 1982.

Carter, N.L., D.W. Baker, and R.P. George Jr., Seismic anisotropy, flow, and constitution of the upper mantle, in *Flow and Fracture of Rocks*, *Geophys. Monogr. Ser.*, edited by H.C. Heard, et al., vol. 16, pp. 167-190, AGU, Washington, D. C., 1972.

Cassard, D., Structure et origine des gisements de chromite du Massif du Sud (ophiolites de Nouvelle Caledonie), Thèse de 3ème Cycle, Univ. Nantes, Nantes, France, 1980.

Chastel, Y.B., P.R. Dawson, H.-R. Wenk, and K. Bennet, Anisotropic convection with implications for the upper mantle, *J. Geophys. Res.*, *98*, 17,757-17,771, 1993.

Christensen, N.I., The magnitude, symmetry and origin of upper mantle anisotropy based on fabric analysis of ultramafic tectonites, *Geophys. J. R. Astron. Soc.*, *76*, 89-112, 1984.

Darot, M., and Y. Gueguen, High-temperature creep of forsterite single crystals, *J. Geophys. Res.*, *86*, 6219-6234, 1981.

Doukhan, N., J.C. Doukhan, J.D. FitzGerald, P.N. Chopra, and M.S. Paterson, A TEM microstructural study of experimentally deformed Anita Bay dunite, in *Deformation of Ceramics II*, edited by R.E. Tressler and R.C. Bradt, pp. 307-319, Plenum, New York, 1984.

Drury, M.R., R.L.M. Vissers, D. Van der Wal, and E.H.H. Strating, Shear localisation in upper mantle peridotites, *Pure Appl. Geophys.*, *137*, 439-460, 1991.

Durham, W.B., and G. Goetze, Plastic flow of oriented single crystals of olivine, 1, Mechanical data, *J. Geophys. Res.*, *82*, 5737-5753, 1977.

Durham, W.B., G. Goetze, and B. Blake, Plastic flow of oriented single crystals of olivine, 2, Observations and interpretations of the dislocation structures, *J. Geophys. Res.*, *82*, 5755-5770, 1977.

Eshelby, J.D., The determination of the elastic field of a ellipsoidal inclusion, and related problems, *Proc. R. Soc. London, Ser. A*, *241*, 376-396, 1957.

Etchecopar, A., A plane kinematic model of progressive deformation in a polycrystalline aggregate, *Tectonophysics*, *39*, 121-139, 1977.

Etchecopar, A., and G. Vasseur, A 3-D kinematic model of fabrc development in polycrystalline aggregates: Comparison with experimental and natural examples, *J. Struct. Geol.*, *9*, 705-717, 1987.

Garcia-San Millan, R.S., Petrofábrica y anisotropía sísmica: Análisis y significado en una sección representativa de la transición corteza-manto subcontinental (Manto de Los Reales, Cordilleras Béticas), Ph.D. thesis, Univ. del Pais Vasco, Bilbao, Spain, 1998.

Goetze, C., and D.L. Kohlstedt, Laboratory study of dislocation climb and diffusion in olivine, *J. Geophys. Res.*, *78*, 5961-5971, 1973.

Green, H.W., and S.V. Radcliffe, Deformation processes in the upper mantle, in *Flow and fracture of rocks*, *Geophys. Monogr. Ser.*, edited by H.C. Heard et al., vol. 16, pp. 139-158, AGU, Washington, D. C., 1972.

Jaroslow, G.E., G. Hirth, and H.J.B. Dick, Abyssal peridotite mylonites: Implications for grain-size sensitive flow and strain localization in the oceanic lithosphere, *Tectonophysics*, *256*, 17-37, 1996.

Jessel, M.W., Simulation of fabric development in recrystallizing aggregates, I, Description of the model, *J. Struct. Geol.*, *10*, 771-778, 1988.

Karato, S., The role of recrystallization in the preferred orientation of olivine, *Phys. Earth Planet. Inter.*, *51*, 107-122, 1988.

Kumazawa, M., and O.L. Anderson, Elastic moduli, pressure derivatives, and temperature derivatives of single-crystal olivine and single-crystal forsterite, *J. Geophys. Res.*, *74*, 5961-5972, 1969.

Kunze, F.R., and H.G. Avé Lallemant, Non-coaxial experimental deformation of olivine, *Tectonophysics*, *74*, T1-T13, 1981.

Lapierre, J., W. Ben Ismail, and D. Mainprice, A method to calculate rock physical properties from published pole figures, in *Structural Geology and Personal Computers*, edited by D.G. De Paor, pp. 167-178, Pergamon, Tarrytown, N. Y., 1996.

Law, R.D., Relationships between strain and quartz crystallographic fabrics in the Roche Maurice quartzites of Plougastel, western Brittany, *J. Struct. Geol.*, *8*, 493-515, 1986.

Lebensohn, R.A., and C.N. Tomé, A self-consistent anisotropic approach for the simulation of plastic deformation and texture development of polycrystals: Application to zirconion alloys, *Acta Metall. Mater.*, *41*, 2611-2624, 1993.

Lloyd, G.E., and B. Freeman, Dynamic recrystallization of quartz under greenschist conditions, *J. Struct. Geol.*, *16*, 867-881, 1994.

Mackwell, S.J., High-temperature rheology of enstatite: Implications for creep in the mantle, *Geophys. Res. Lett.*, *18*, 2027-2030, 1991.

Mackwell, S.J., D.L. Kohlsted, and M.S. Paterson, Role of water in the deformation of olivine single-crystals, *J. Geophys. Res.*, *90*, 11,319-11,333, 1985.

Mainprice, D., A FORTRAN program to calculate seismic anisotropy from the lattice preferred orientation of minerals, *Comput. Geoscii.*, *16*, 385-393, 1990.

Mainprice, D., and P.G. Silver, Interpretation of SKS-waves using samples from the subcontinental lithosphere, *Phys. Earth Planet. Inter.*, *78*, 257-280, 1993.

Mainprice, D., W. Ben Ismail, G. Barruol, A. Vauchez, and J. Boyd, Mantle root anisotropy of the Kaapval craton (South Africa) from lattice preferred orientation analysis (abstract), *Eos, Trans. AGU*, *78 (46)*, Fall Meet. Suppl., F471, 1997.

Mercier, J.-C., and A. Nicolas, Textures and fabrics of upper mantle peridotites as illustrated by xenoliths from basalts, *J. Petrol.*, *16*, 454-487, 1975.

Mockel, J.R., The structural petrology of the garnet peridotite of Alpe Arami (Ticino, Switzerland), *Leidse Geol. Meded.*, *42*, 61-130, 1969.

Molinari, A., G.R. Canova, and S. Azhy, A self-consistent approach of the large deformation crystal polycrystal viscoplasticity, *Acta Metall.*, *35*, 2983-2994, 1987.

Nicolas, A., *Structures of Ophiolites and Dynamics of Oceanic Lithosphere*, 367 pp., Kluwer Academic Publishers, Norwell, Mass., 1989.

Nicolas, A., and N.I. Christensen, Formation of anisotropy in upper mantle peridotites: A review, in *Composition, Structure and Dynamics of the Lithosphere-Asthenosphere System, Geodyn. Monogr. Ser.*, edited by K. Fuchs and C. Froidevaux, pp. 111-123, AGU, Washington, D. C., 1987.

Nicolas, A., and J.P. Poirier, *Crystalline Plasticity and Solid State Flow in Metamorphic Rocks*, 444 pp., John Wiley, London, 1976.

Nicolas, A., J.L. Bouchez, F. Boudier, and J.C. Mercier, Textures, structures and fabrics due to solid state flow in some European lherzolites, *Tectonophysics*, *12*, 55-86, 1971.

Nicolas, A., F. Boudier, and A.M. Boullier, Mechanism of flow in naturally and experimentally deformed peridotites, *Am. J. Sci.*, *273*, 853-876, 1973.

Parks, D.M., and S. Ahzi, Polycrystalline plastic deformation and texture evolution for crystals lacking five independent slip systems, *J. Mech. Phys. Solids*, *38*, 701-724, 1990.

Phakey, P., G. Dollinger, and J. Christie, Transmission electron microscopy of experimentally deformed olivine crystals, in *Flow and fracture of rocks*, *Geophys. Monogr. Ser.*, edited by H.C. Heard et al., vol. 16, pp. 117-138, AGU, Washington, D. C., 1972.

Poirier, J.P., and A. Nicolas, Deformation-induced recrystallization due to progressive misorientation of subgrains, with special reference to mantle peridotites, *J. Geol.*, *83*, 707-720, 1975.

Raleigh, C.B., Mechanisms of plastic deformation of olivine, *J. Geophys. Res.*, *73*, 5391-5407, 1968.

Ribe, N.M., A continuum theory for lattice preferred orientations, *Geophys. J. R. Astron. Soc.*, *97*, 199-207, 1989.

Ribe, N.M., and Y. Yu, A theory for plastic deformation and textural

evolution of olivine polycrystals, *J. Geophys. Res.*, *96*, 8325-8335, 1991.

Russo, R.M., and P.G. Silver, Trench-parallel flow beneath the Nazca plate from seismic anisotropy, *Science*, *263*, 1105-1111, 1994.

Schärmeli, G.H., Anisotropy of olivine thermal conductivity at 2.5 GPa and up to 1500K measured on optically non-thick samples, in *High-Pressure Researches in Geosciences*, edited by W. Schreyer, pp. 349-373, Schweizerbart, Stuttgart, Germany, 1982.

Schmid, S.M., R. Panozzo, and S. Bauer, Simple shear experiments in calcite rocks: Rheology and microfabric, *J. Struct. Geol.*, *9*, 747-778, 1987.

Seront, B., Déformation expérimentale à haute pression et temperature d'agrégats polycrystallins de plagioclase et olivine, Ph.D. thesis, Université de Montpellier II, 1993.

Silver, P.G., and W. Chan, Implications for continental structure and evolution from seismic anisotropy, *Nature*, *335*, 34-39, 1988.

Skrotzki, W., A. Wedel, K. Weber, and W.F. Muller, Microstructure and texture in lherzolites of the Balmuccia massif and their significance regarding the thermomechanical history, *Tectonophysics*, *179*, 227-251, 1990.

Takeshita, T., Plastic anisotropy in textured mineral aggregates: Theories and geological implications, in *Rheology of Solids and of the Earth*, edited by S. Karato and M. Toriumi, pp. 237-283, Oxford Univ. Press, New York, 1989.

Takeshita, T., H.-R. Wenk, A. Molinari, and G. Canova, Simulation of dislocation-assisted plastic flow in olivine polycrystals, in *Deformation Processes in Minerals, Ceramics, and Rocks*, edited by J.D. Barber and P.G. Meredith, pp. 365-377, Hyman, London, 1990.

Taylor, G.I., Plastic strain in metals, *J. Inst. Met., 62*, 301-324, 1938.

Tiem, S., M. Berveiller, and G.R. Canova, Grain shape effects on the slip system activity and on the lattice rotation, *Acta Metall. Mater.*, *34*, 2139-2159, 1986.

Tomé, C.N., and G. Canova, Self-consistent modeling of heterogeneous plasticity, in *Texture and Anisotropy Preferred Orientations in Polycrystals and Their Effect on Mechanical Properties*, edited by U.F. Kocks, C.N. Tomé, and H.-R. Wenk, 675 pp., Cambridge Univ. Press, New York, 1998.

Tommasi, A., Forward modeling of the development of seismic anisotropy in the upper mantle, *Earth Planet. Sci. Lett.*, *160*, 1-13, 1998.

Tommasi, A., B. Tikoff, and A. Vauchez, Upper mantle tectonics: Three-dimensional deformation, olivine crystallographic fabrics and seismic properties, *Earth Planet. Sci. Lett.*, *168*, 173-186, 1999.

Toriumi, M., and S. Karato, Preferred orientation development of dynamically recrystallized olivine during high-temperature deformation, *J. Geol., 93*, 407-417, 1985.

Urai, J.L., W.D. Means, and G.S. Lister, Dynamic recrystallization of minerals, in *Mineral and Rock Deformation: Laboratory Studies*, edited by B.E. Hobbs and H.C. Heard, pp. 161-199, AGU, Washington, D. C., 1986.

Van der Wal, D., Deformation processes in mantle peridotites, Ph.D. thesis, Rijksuniversiteit Utrecht, Utrecht, Netherlands, 1993.

Vauchez, A., and G. Barruol, Shear waves splitting in the Appalachians and the Pyrenees: Importance of the inherited tectonic fabric of the lithosphere, *Phys. Earth Planet. Inter.*, *95*, 127-138, 1996.

Vinnik, L.P., G.L. Kosarev, and L.I. Makeyeva, Anisotropy of the lithosphere from the observations of SKS and SKKS, *Proc. Acad. Sci. USSR Geol. Sci. Sect., Engl. Transl., 78*, 1335-1339, 1984.

Wenk, H.-R., K. Bennet, G.R. Canova, and A. Molinari, Modelling plastic deformation of peridotite with the self-consistent theory, *J. Geophys. Res.*, *96*, 8337-8349, 1991.

Wenk, H.-R., G.R. Canova, Y. Brechet, and L. Flandin, A deformation-based model for recrystallization of anisotropic materials, *Acta Metall. Mater.*, *45*, 3283-3296, 1997.

Zhang, S., and S. Karato, Lattice preferred orientation of olivine aggregates in simple shear, *Nature*, *375*, 774-777, 1995.

Zhang, Y., B.E. Hobbs, and A. Ord, A numerical simulation of fabric development in polycrystalline aggregates with one slip system, *J. Struct. Geol.*, *16*, 1297-1313, 1994.

Y. Chastel, CEMEF, Ecole de Mines de Paris, 06904 Sophia Antipolis, France. (Yvan.Chastel@cemef.cma.fr)

D. Mainprice and A. Tommasi, Laboratoire de Tectonophysique, ISTEEM, CNRS/Université de Montpellier II, 34095 Montpellier cedex 5, France. (david@dstu.univ-montp2.fr; deia@dstu.univ-montp2.fr)

(received February 2, 1999; revised November 2, 1999;
accepted November 11, 1999)

[1] Deceased July, 28 1997.

Paper number 1999JB00411.
0148-0227/00/1999JB900411$09.00

JOURNAL OF GEOPHYSICAL RESEARCH – SOLID EARTH, 105 (B4): 7893-7908